Advances in Science and Technology Research Journal

Advances in Science and Technology Research Journal, 2026, 20(7), 438–453
https://doi.org/10.12913/22998624/218557
ISSN 2299-8624, License CC-BY 4.0

Received: 2026.01.05
Accepted: 2026.05.15
Published: 2026.06.01

AI-driven multi-parameter optimization of high-performance epoxy composites for tribological applications

Huda Fadol S Alyafei[1], Ahmed Nabhan[2,3], Mohamed Taha[4*], Ameer A. Kamel[2], Esraa M. Abd Elsadek[4]

[1] Department of Physics and Materials Sciences, College of Arts and Sciences, Qatar University, Doha, Qatar
[2] Production Engineering and Mechanical Design, Faculty of Engineering, Minia University, El-Minia 61111, Egypt
[3] Mechatronics Program, Faculty of Engineering, Minia National University, El-Minia, 61519, Egypt
[4] Mechanical Engineering Department, College of Engineering and Technology, Arab Academy for Science, Technology and Maritime Transport, Sadat Road - P.O. Box 11, Aswan, Egypt
* Corresponding author's e-mail: mohamed_taha@aast.edu

ABSTRACT

Epoxy composites reinforced with a hybrid nanofiller consisting of paraffin oil (PO) and Al_2O_3 nanoparticles demonstrate enhanced mechanical and tribological performance for frictional applications. This study investigates the influence of Al_2O_3 NPs loading (0.5–2.0 wt.%) combined with 5 wt.% PO on hardness, compressive yield strength, elastic modulus, coefficient of friction, and wear resistance, supported by three-dimensional surface topography and scanning electron microscopy analyses of worn surfaces. The results indicate that an optimal balance between reinforcement and lubrication is achieved at low nanoparticle loading (1.0 wt.% Al_2O_3 NPs), where improved filler dispersion enhances load transfer and reduces surface damage. Significant reductions in friction and wear were observed, with decreases of approximately 43% and 34%, respectively, compared with neat epoxy. At higher loadings, (≥1.5 wt.% Al_2O_3), particle agglomeration influences deformation and frictional behavior. Furthermore, an adaptive neuro-fuzzy inference system (ANFIS) model shows strong agreement with experimental results, enabling reliable prediction of composite performance based on composition and processing variables. These findings highlight the effectiveness of combining hybrid nanofillers with AI-assisted modeling for optimizing epoxy composites in tribological applications.

Keywords: epoxy nanocomposites, aluminum oxide nanoparticles, paraffin oil, tribological performance, self-lubricating composites, modeling.

INTRODUCTION

Epoxy resin has served as a prominent thermosetting polymer for over five decades due to its exceptional structural integrity, durability, chemical resistance, production efficiency, and large-scale availability [1]. Thermal-cured epoxy resins are widely used in structural engineering applications. Therefore, understanding the mechanics and mechanisms of fracture of these materials is of vital importance [2]. Resins are categorized as special resins because of their unique properties, including minimal shrinkage during curing, nonvolatile treatment, compatibility with various materials, exceptional durability and strength, strong adhesion, and resistance to rust, chemicals, and electricity [3]. Epoxy resins provide a web of treatments using various therapeutic substances, such as amines, anhydrides, petioles [4]. Epoxy has a wide range of chemical and processing uses, including protective coatings, colors, adhesives, electronics, industrial blocks, and composites [2]. The dynamic mechanical characteristics and wear resistance of polymer matrices are impacted by the introduction of fumed silica [5], TiC NPs [6], and graphene nanofillers [7]. Iron dust was employed

as a filler for epoxy flooring to increase the COF and lower electrostatic charges coming from shoe friction with the floor under dry [8] and wet slippery scenarios [9]. Examining the mechanism of self-lubrication contributes to the formulation of polymeric structures with superior frictional performance under varied operating scenarios [10].

Oil and grease, as well as thin film coatings and gases (like air bearings), are good enough for lubrication [11]. Plant-based oils were carried out as a thickening of lithium soap to boost performance [12]. It was depicted that a loading dose of 0.01 wt% of reduced graphene dispersion with paraffin grease leads to COF and mass loss up to 50% and 85% reduction, in order [13]. The physical, chemical and tribological properties of lithium soap coupled with soybean oil [14], castor and coconut oils [15] were examined. Nanoparticles and submicron particles are two examples of beneficial lubricant additives that can improve tribological properties [16]. CeO_2 and polytetrafluoroethylene NPs were dispersed with castor oil. It was discovered that the wear scar diameter diminishes approximately 37% and 35% at a loading dose of 0.25% wt% of CeO_2 and PTEF NPs, in order [17]. Al_2O_3 NPs and CNC were added to gear oil [18], Al_2O_3 NPs and MWCNTs were incorporated into engine oil [19], and CNC was put into spent oil [20] to evaluate under operating conditions. It was indicated that a loading level of 0.5 wt% of MoS_2 dispersion with liquid paraffin leads to COF [21].

Sustainable polymers made from organic oils are touted as a stable, long-term replacement for petroleum-based polymers [22]. The chemical composition of triglycerides may be a suitable approach for creating resins, polyurethanes, polyester, and epoxy systems with scalable and adjustable features [23]. These polymers are biodegradable, have a minimal carbon footprint, and are consistent with green chemistry concepts [24]. A useful component of the process is life cycle assessment or other sustainability criteria, such as utilizing ISO standards to evaluate biodegradability [25]. The structural modification approaches open prospects in a wide range of fields, including coatings, adhesives, packaging, and biomedicine [26]. Furthermore, organic oil-based polymers provide a practical approach toward a circular economy and the construction of environmentally benign goods [27]. The impacts of reinforcing epoxy with carbon nanotubes and filling it with different types of plant-based oils on the COF were explored. It was indicated that with the amount of CNTs at 0.6% by weight and with maize oil, the COF reduction level was 93% [28].

Numerous research has demonstrated that nanocomposites have superior mechanical and thermal properties over traditional composites [29]. Upgrading the performance of epoxy matrix composites employing nanoparticles such as Al_2O_3 [30], SiO_2 [31], TiO_2 [32], CNTs [33], GNPs [34], hybrid SiC/TiO_2 [35], hybrid nanofiller GNPs/Al_2O_3 [36], and other types is currently attracting an immense amount of attention [37]. Al_2O_3 NPs enhance the hardness and surface damage resistance of the epoxy matrix, thereby increasing its load-bearing capacity [38]. Integrating SiO_2 NPs into epoxy resin strengthens structural integrity, stress distribution and crack resistance [39]. GNPs strengthen barrier attributes, thermal conductivity, and friction lowering due to creating a multi-layered structure that prevents crack propagation and promotes lubrication [40]. The GNPs/Al_2O_3 hybrid filler improves stiffness, reduces friction, and increases the durability of epoxy formulations [41]. It was noticed that incorporating nanosized fillers, as opposed to the more common micrometer-sized fillers, may represent an effective way towards improving the thermal and mechanical attributes of thermoset resins [42]. Plant-based oils exhibit a unique precursor to synthetic of bio-epoxy composites due to their availability, biodegradability, and the presence of the functional groups [43]. It may be obvious that PO is frequently incorporated with epoxy matrices to control the flexibility, hydrophobicity, and phase stability of epoxy formulations [44]. Molten paraffin wax and asphaltene expanded the viscosity of the epoxy matrix when it hardened. This was the case even though it did not hinder bonding or lower the produced polymer's glass transition point [45]. The results show that dispersion of 3% by weight of hydrophobic silica NPs with epoxy exhibits higher contact angles (100–110°). Furthermore, the dispersion of the silica NPs and the paraffin wax content control the high corrosion resistance of the composites [46]. Moreover, castor oil contains high content of ricinoleic acid - rich in hydroxyl groups- which can be utilized to directly manufacture polyols and epoxy networks [47] and epoxy networks [48]. Most thermoset hybrids that are employed particularly regularly are epoxy/clay nanocomposites [49]. The incorporated Al_2O_3 NPs through oil-epoxy system performs to enhance thermal stability, mechanical

strength, and wear resistance [50]. Hydrophobic epoxy coatings were prepared on different surfaces by utilizing hydrophobized Al_2O_3 NPs. It was found that the corrosion resistance of the galvanized and skin-passed galvanized surfaces increased with a high loading level of Al_2O_3 NPs [51]. Furthermore, other nanofillers like graphene, SiO_2, or h-BN are employed to add multifunctional properties including lubricity, conductivity, and flame resistance [52]. For energy-related, automotive, and aerospace applications, the bio-epoxy nanocomposites offer exceptional durability and reduce reliance on petroleum resources. Epoxy/clay nanocomposites based on castor oil have been shown to have increased hardness and thermal stability [53]. Moreover, epoxy systems based on palm ash exhibit modified thermal stability and increase in cross-linking [54]. On the other hand, paraffin wax contents of silica NPs embedded into epoxy formulations improve corrosion resistivity and maximize salt spray resistances [55].

Recently, artificial intelligence methods, especially predictive modeling techniques, have demonstrated their ability to represent complex nonlinear connections and monitor the behavior of composite materials [56]. Artificial neural networks (ANNs) were evaluated for their prediction and performance in modeling bio/synthetic epoxy hybrids' physical, mechanical, and thermal properties [57]. Optimized ANNs were applied to predict the dynamic viscosity of zinc oxide-containing nano-lubricants in commercial oils. The results revealed good agreement between the actual and predicted ANNs values for simulating the performance of the synthetic composite [58]. The adaptive neurowaszy inference system (ANFIS) and response surface methodology (RSM) were used to calibrate and predict the dry sliding wear response of AlMg1SiCu/silicon carbide/molybdenum disulfide hybrid composites. The neural network model in the ANFIS backpropagation algorithm was trained using the output responses to weight loss. The ANFIS model data revealed more accurate responses compared to the RSM model for predicting the wear state of the hybrid composite surface [59]. The tribological performance and mechanical behavior of HDPE/graphene nanocomposites were predicted using ANFIS models [60]. The ANFIS model responses revealed their ability to predict tribological and mechanical properties with an error of less than 3%. A review of epoxy composites has revealed a wide range of applications due to the unique properties of the composite. Nevertheless, the integration of Al_2O_3 NPs with PO remains insufficiently explored in the literature despite the unique qualities of each. Therefore, this work aims to optimize epoxy/PO/ Al_2O_3 nanocomposites for tribological applications using coupled experimental characterization and adaptive neuro-fuzzy inference system ANFIS-based predictive modeling. This combined experimental–computational framework offers new insights into designing multifunctional epoxy composites for advanced tribological applications.

In the subsequent portions, the methodology employed, the results achieved, and the implications of our findings are presented.

MATERIALS AND PROCEDURES

Materials

In this current study, epoxy resin was confirmed as the base material for the synthesis of a highly efficient friction composite. More specifically, KEMAPOXY 150 epoxy resin, purchased from CMB Group in Egypt, was employed. The two main constituents of KEMAPOXY 150 epoxy substance are component A, which is the resin, and component B, which is the hardener. The epoxy resin has excellent physical properties, with a density of 1.11 g/cm³ and a tensile load capacity of 150–250 kg/cm³. Moreover, it may withstand temperatures of up to 140°C in dry conditions and 90 °C in wet environments. The hybrid nanofillers, composed of PO and aluminum oxide (Al_2O_3) nanoparticles, were integrated into the epoxy matrix to evaluate its framework performance and functional qualities. The Al_2O_3 NPs, acquired from US Research Nanoparticles, demonstrate an extraordinarily high purity level of 99.9%, assuring minimal contamination that could otherwise alter the composite's performance. These nanoparticles are spherical in shape with an average particle size ranging from 40 to 50 nm, an effective density of 3890 kg/m³, a mass density of 0.18 g/mL, and a surface area of approximately 35 m²/g. This facilitates homogeneous dispersion throughout the epoxy matrix and increases interfacial adhesion. The oil's low viscosity and hydrophobic properties increase the filler's compatibility with the matrix, which may boost processability, and potentially lower the brittleness of the cured epoxy structure.

Samples preparation

Epoxy-based samples were developed through a series of regulated processes to ensure uniform dispersion of the hybrid nanofillers interior the matrix, as illustrated in Figure 1. Starting out, the basic resin was assessed by integrating component A (epoxy resin) with component B (hardener) at a constant weight distribution of two-to-one. The blending process was conducted at 300 rpm for a duration of 5 minutes to obtain a homogeneous base system. In the second step, PO containing dispersed Al_2O_3 NPs was prepared. For this purpose, Al_2O_3 NPs with loading contents (0.5, 1.0, 1.5, and 2.0% by fracture weight) were added to the PO at a constant loading of 5.0% by fracture weight. The mixture was integrated utilizing mechanical stirring at rotating speed 500 rpm for 15 minutes - Dihan HG-15 stirrer, Vietnam- under ambient experimental settings (30 °C, 55% relative humidity). subsequently, the hybrid nano-oil suspension was incorporated with the epoxy matrix, and the resulting mixture was homogenized by mechanical stirring at 300 rpm for a duration of 10 minutes. Finally, to reduce nanoparticle agglomeration and achieve improved homogeneity, the mixtures were ultrasonicated using a Dihan WUC-A03 ultrasonic processor (Vietnam) for a duration of 20 minutes. The prepared samples were then labeled according to their compositions, as shown in Table 1.

Table 1. The sample labels and their varied incorporation concentrations

Sample labels	Epoxy	PO	Al_2O_3 NPs
Epoxy Neat	100%	-	-
Epoxy NC1	95%	5%	-
Epoxy NC2	94.5%	5%	0.5%
Epoxy NC3	94%	5%	1.0%
Epoxy NC4	93.5%	5%	1.5%
Epoxy NC5	93%	5%	2.0%

ANFIS MODEL

The ANFIS integrates fuzzy logic with artificial neural networks to depict nonlinear relationships between components. Fuzzy logic turns qualitative input into quantitative outputs, whereas neural networks permit adaptive change of membership functions for enhanced prediction accuracy. The framework was constructed using the MATLAB Adaptive Neuro-Fuzzy toolbox, allowing simplifies the building, training, and assessment of Sugeno-type fuzzy constructions.

ANFIS structures were used in this study, as shown in Figure 2. The first ANFIS design includes a single output and a six input, which are the mechanical characteristics of the epoxy nanocomposites and their different incorporation concentrations. For this specific construction,

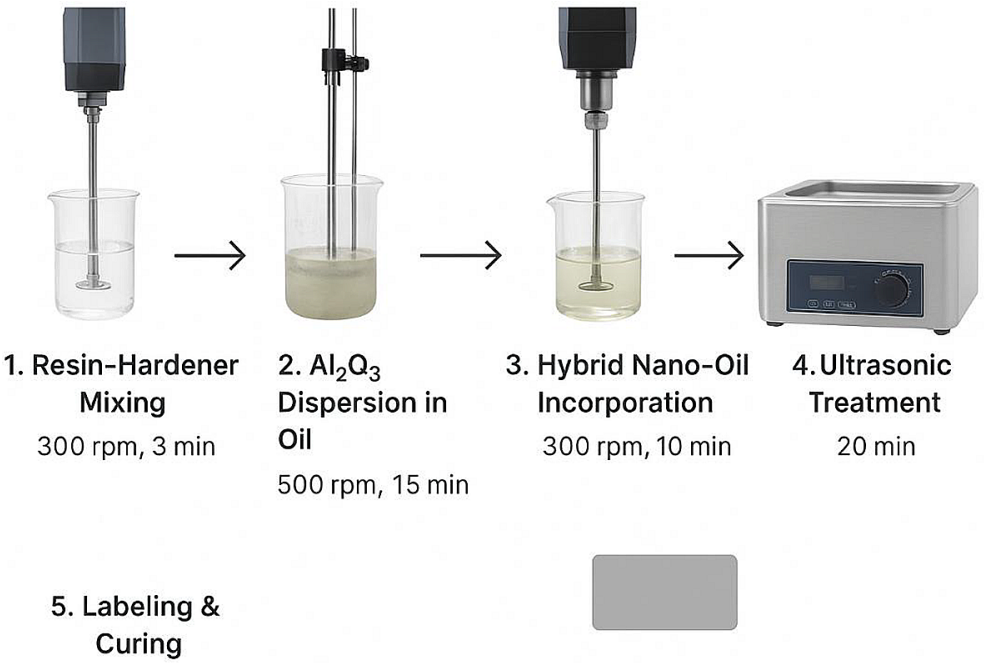

Figure 1. A schematic of sample preparation procedure

four ANFIS models were developed, each of which corresponded to one of the following outputs: normal load, vibration to load speed, sliding distance, or rotational speed. Furthermore, there is just one output from this structure. For the provided structure, four different ANFIS models were created, each of which was particularly made to estimate the sliding distance or the COF. The ANFIS framework comprises of five layers that jointly execute fuzzification, rule evaluation, normalization, defuzzification, and output creation. In the fuzzification layer, membership functions translate numerical inputs into linguistic parameters. The rule layer examines the firing strength of fuzzy rules, followed by normalization to ensure balanced contribution of each rule. The defuzzification procedure subsequently turns fuzzy outputs into crisp values, and the last layer produces the projected response. A hybrid learning approach incorporating least-squares estimation and backpropagation was utilized to train the model using experimental input–output datasets.

The ANFIS framework explains the interplay between nanofiller loading, material characteristics, and operating circumstances. It reveals that enhanced nanoparticle dispersion promotes load transfer, whereas PO helps to lubrication through protective film development. It also implies that excessive filler content can lead to agglomeration and poor performance. Therefore, the model not only delivers correct predictions but also supports comprehension of the systems regulating mechanical and tribological function.

EXPERIMENTS DETAILS

Structure analysis

The structural, strength-related, and surface interaction characteristics of epoxy nanocomposites were investigated using different methodologies. In this study, IR spectroscopy was used to identify the harmonic components of the interaction bonds in the epoxy matrix. The examination was conducted utilizing a Beckman IR 4250 spectrometer (USA), working inside the IR area, comprising wavenumbers that vary from 400 to 4000 cm^{-1}, and evaluating transmittance (%). The crystalline structure and phase recognition of the epoxy matrices were evaluated utilizing a Siemens D500 X-ray diffractometer (German). The analysis using XRD was carried out with an experimental arrangement of 30 mA electricity and 30 kV amplitude over a measurement interval ranging from 0° to 70° of (2θ).

Mechanical characterizations

The mechanical responses were analyzed to determine the yield strength, elastic modulus, breaking stress percentage, and hardness. Uniaxial universal testing was done on the epoxy nanocomposites using a DFM-300KN apparatus from China, following the requirements of ASTM D1621. The evaluation of hardness was carried out using a Durometer apparatus, namely Shore D, in conformity with the standards of ASTM

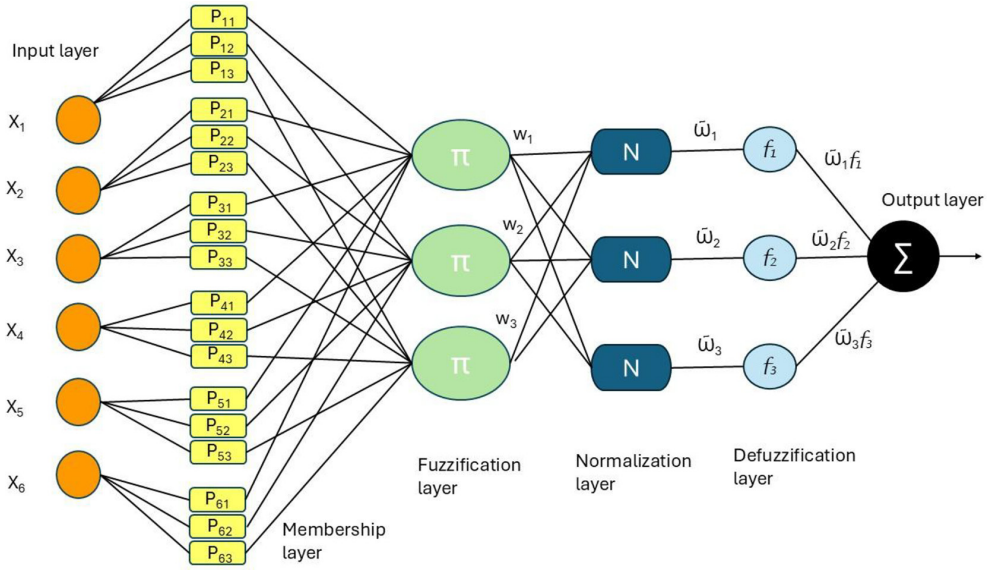

Figure 2. ANFIS structure: Tribological and mechanical models

D2240. Five different positions were employed for the hardness test, and any differences were averaged out.

To evaluate the level of nanocomposite production quality, sample densities were computed. For every quantity of filler, both experimental and theoretical densities were identified. The following formula can be used to calculate the theoretical density of the composite given the mass ratio and filler quantity of each component:

$$\rho_{Th} = \frac{1}{(w_E/\rho_E + w_{PO}/\rho_{PO} + w_A/\rho_A)} \quad (1)$$

where: w_E, w_{PO} and w_A are concentrations level of epoxy substance, PO and Al_2O_3 NPs, respectively. ρ_E, ρ_{PO} and ρ_A are the densities of ingredients in the same sequence as previously stated. The Archimedes principle can be employed to establish the samples' real density based on ASTM D792. The succeeding equation was adopted to compute the mass of the samples in air and water, two alternative media:

$$\rho_E = \frac{w_{s-air}}{w_{s-air} - w_{s-water}} \quad (2)$$

where: the weights of the samples on each medium are denoted by $w_{s\text{-}air}$ and $w_{s\text{-}water}$. The results of theoretical and experimental density calculations can then be compared to determine the void volume fraction.

$$v_v = \frac{\rho_{Th} - \rho_E}{\rho_{Th}} \quad (3)$$

Tribological attributes

A sliding-contact evaluation setup was employed to quantify the wear and friction response in accordance with ASTM standard G99-95 guidelines. The samples were examined in dry conditions with an ambient temperature of 30 °C and an approximate humidity of 60%, rubbing across a stainless-steel alloy disk. Frictional response, expressed as the COF, was recorded across an applied load of 2–10 N while maintaining a uniform sliding speed of 0.1 m/s. In addition, the evaluation of weight reduction was conducted by use of an indenter that moved over the sample surfaces at intervals of 31.4, 47.1, 62.8, 94.2, and 125.6 m while being loaded with 10 N. To determine the weight loss (Δm, in grams), the samples were weighed both before and after testing. The wear rate (W_R) was calculated by applying the formula supplied:

$$W_R = \frac{\Delta m}{L\ \rho\ F_n} \quad (4)$$

The analysis incorporated key inputs, which were normal applied load (F_n), sample density (ρ), and sliding-contact distance (L). For detailed topological assessment, the surface morphology of the worn regions was investigated through optical microscopy (OLYMPUS BX53M, Japan) and SEM (JEOL JCM-6000Plus, Japan).

RESULTS AND DISCUSSION

The crystal structure of the epoxy matrix, augmented with PO and Al_2O_3 NPs as hybrid nanofillers, was examined using IR spectroscopy and XRD methods. Figure 3a shows the samples of epoxy nanocomposite investigation using IR spectra. The information gleaned from these spectra made it easier to evaluate how the epoxy resin and hybrid nanofiller interacted. The methyl group, symmetric methylene and methine sets of the oxirane band, and the CH_2 group next to the oxirane band all exhibit C–H stretching in pure epoxy, as seen by the peaks seen at 2861, 2989, and 3312 cm^{-1}. Vibrational peaks at 1604 and 1469 cm^{-1} may also be identified to the aromatic moiety's C=C bonds being stretched. Intermolecular hydrogen bonding causes the hydroxyl group to show up as a peak at 3347 cm^{-1}, exhibiting a wider nature. In addition, the oxirane ring exhibits its typical peak at 1165 and 813 cm^{-1}. The relatively diminished intensity of these peaks results from the low concentration of Al_2O_3 NPs in the matrix [61], [62] NPs in the matrix [61], [62]. This finding implies that the oxirane moiety's ring opening, which created a cross-linked network, had in fact caused the curing process to occur. Subsequently, IR spectra were collected from the epoxy nanocomposite samples, and the outcomes clearly affirmed that these samples preserved identical functional group bands as the pristine sample. These results provide conclusive evidence regarding the effective integration of hybrid nanofillers into the epoxy matrix.

XRD was utilized to peer into the materials' crystalline phases. In this study, we compared different weight percentages of Al_2O_3 NPs. Through XRD analysis, we aimed to discern whether reinforcing the epoxy system with Al_2O_3 NPs altered

their crystalline structure during the creation of the hybrid PO and Al_2O_3 NPs solution or during the subsequent curing and drying processes [63]. As illustrated in Figure 3b, A widened peak exhibiting characteristics of amorphous epoxy halo may be seen in the XRD assessment plot, wavelength angle (2θ) spans between 10° to 30°. However, the composite showed a discernible increase in intensity when hybrid paraffin oil and Al_2O_3 NPs were incorporated to the pure epoxy matrix [64]. These observed results align with the information documented in existing literature, suggesting that the polymer chains within the composite are either cross-linked or integrated into the hybrid paraffin oil and Al_2O_3 NPs phase by hydrogen and covalent bonding [65].

Theoretical findings, depicted in Figure 4a, indicate an augmentation in density values corresponding to increased filler loading. However, the experimental results consistently yielded values lower than the theoretical predictions for various samples. The primary cause of this discrepancy is the voids that emerge during the mixing process. Furthermore, the presence of these voids exerts an influence on various material properties, with their absence signifying the effectiveness and calibre of the blending procedure, as elucidated in Figure 4b. The experimental observations unveiled that the density was enhanced by the incorporation of hybrid PO/Al_2O_3 NPs. Consequently, the sample preparation process was deemed acceptable, as the calculated void volume fraction did not surpass 2.6% [66]. With respect to this, the density of the sample containing the hybrid nanoparticles, denoted as epoxy NC3, exhibited an increase of up to 1.2%. Additionally, elevating the void fraction within the epoxy nanocomposites elevates the likelihood of moisture absorption, might contribute to the degradation of the material's durability [67]. As a result, porosity volume fraction is a common metric used by researchers to assess the quality of composites; a smaller porosity volume

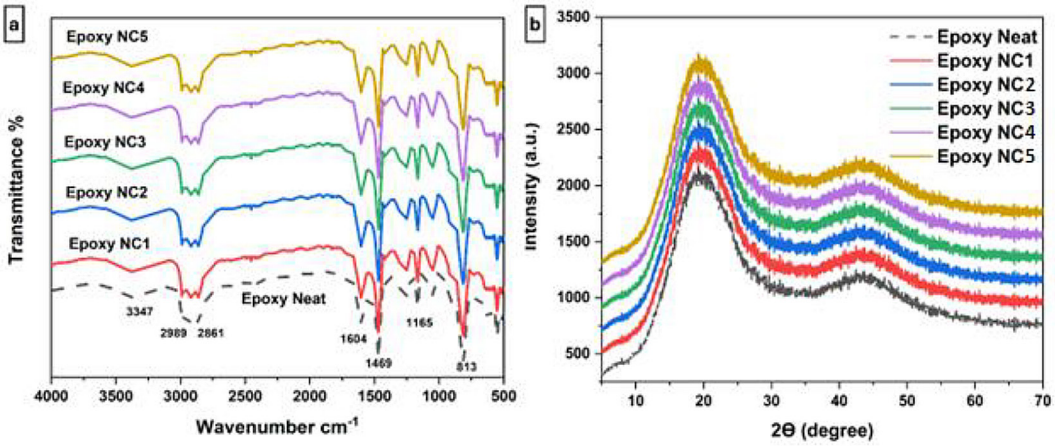

Figure 3. (a) IR spectral response, (b) XRD diffractograms of epoxy nanocomposites

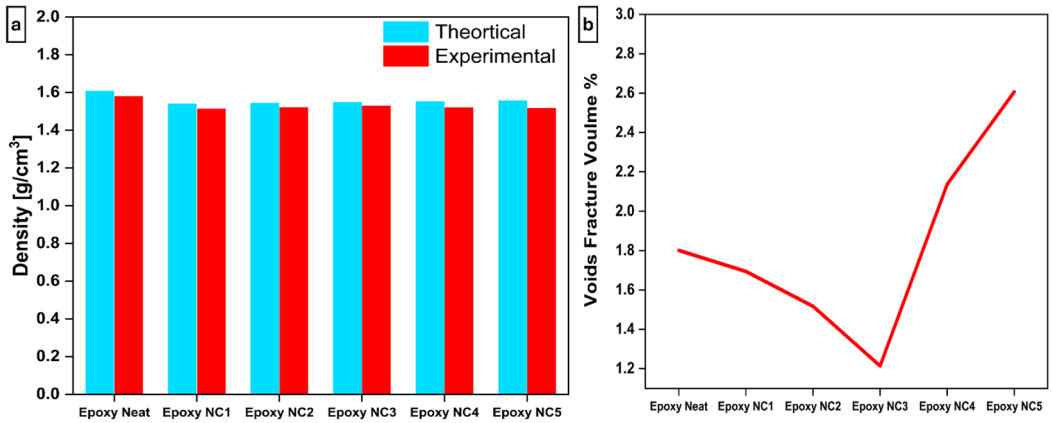

Figure 4. (a) Epoxy nanocomposite sample densities, both theoretical and experimental, (b) voids fracture % of epoxy nanocomposite samples

fraction indicates higher composite quality [68], [69]. To circumvent issues stemming from voids, it is advantageous to mix the composite constituents within a vacuum chamber [70]. Because it might have a potential impact on the attributes of the composites, the porosity volume fraction was calculated for each one, as depicted in Figure 4b. Nano-alumina inclusion is responsible for the reduced porosity volume fraction, which exerted no adverse effects on the cohesion among the molecules of epoxy. Conversely, the alumina modulator strengthens the bond between the nano pigments and the epoxy monomer.

The mechanical characteristics of epoxy nanocomposite specimens were assessed through hardness, tensile strength and elastic modulus, tests. Figure 5a illustrates the Shore hardness values for epoxy nanocomposite specimens. Neat epoxy displayed an average hardness of 78 on the D-index scale. It was observed that hardness exhibited a proportional increase with the rising loading amount of hybrid filler. Specifically, the hardness value experienced a 10.9% boost with a 1.0 wt. % Al_2O_3 NPs loading, as seen in epoxy NC3, in comparison to pure epoxy, achieving a value of 86.5 on the shore D-index. The heightened hardness of the composite may be ascribed to the favorable bonding established between the epoxy matrix and the hybrid filler PO/Al_2O_3 NPs, which facilitates efficient load transfer. Furthermore, the rise in hardness indicates the presence of a homogenous dispersion of Al_2O_3 NPs inside the resin matrix, since the hardness of the composition is dictated by the molecular bonds between the nanoparticles and the epoxy matrix [65]. Furthermore, raising the nanoparticle loading to 1.0 wt.% diminished interparticle spacing while enhancing adhesive linking, thus endowing the composite with significant indentation resistance. These findings indicate that, despite employing a low loading of hybrid filler PO/ Al_2O_3 NPs, the epoxy composite's hardness was enhanced [66].

A compression test was carried out to evaluate the produced epoxy nanocomposites' load-bearing capability and inquire about the improved compressive capabilities associated with the integration of hybrid filler PO/Al_2O_3 NPs that had minimal loading in the matrix of epoxy. Elastic modulus and yield strength were estimated, as shown in Figures 5b. The highest loading content exhibited the most substantial enhancements in yield strength and elasticity modulus, demonstrating about 33.6% and 10% improvements, respectively. It demonstrates that fillers contributed to augmenting the malleability and strain capacity of the epoxy matrix. An overview of the mechanical parameters of epoxy nanocomposites regarding the free epoxy matrix, as presented in Table 2. When the weight fraction of the hybrid filler PO/Al_2O_3 NPs rose, the breaking strain percentage of the epoxy composites also increased. Neat epoxy had a breaking strain of 7.2% ± 0.2, which increased by 23.6% for a level content of 1.0% by weight of Al_2O_3 NPs, such as epoxy NC3, reaching 8.9% ± 0.3. Furthermore, the epoxy matrix chains' mobility hindered by the alumina nanoparticles, increasing the composite's yield strength, elasticity modulus, and breaking strain percentage.

According to ASTM G99-95, the wear rate and COF of epoxy nanocomposites were evaluated. Figure 6a shows changes in the COF with respect to typical loads utilized for different hybrid

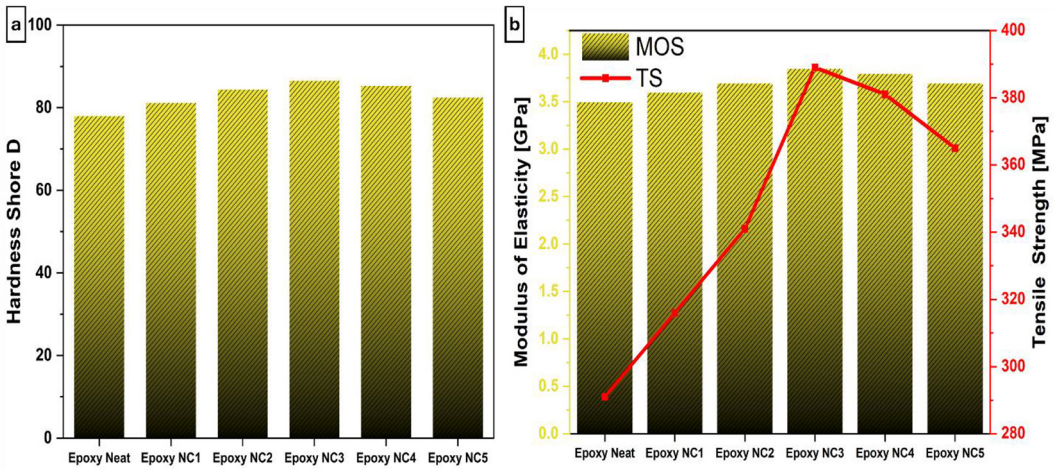

Figure 5. (a) Shore D hardness, (b) elastic modulus, and yield strength evaluation of epoxy nanocomposite samples

Table 2. The epoxy nanocomposites' mechanical properties

Sample No	Yield strength [MPa]	% Improvement	Elastic modulus [MPa]	% Improvement	Breaking strain %	% Improvement
Epoxy Neat	291 ± 4	-	3.5 ± 0.03	-	7.2 ± 0.2	-
Epoxy NC1	316 ± 3	+8.6%	3.6 ± 0.015	+2.9%	7.9 ± 0.15	+9.7%
Epoxy NC2	341 ± 5	+17.2%	3.7 ± 0.02	+5.7%	8.5± 0.25	+18.1%
Epoxy NC3	389 ± 6	+33.7%	3.85 ± 0.01	+10.0%	8.9 ± 0.3	+23.6%
Epoxy NC4	381 ± 5	+30.9%	3.8 ± 0.02	+8.6%	8.7 ± 0.3	+20.8%
Epoxy NC5	365 ± 4	+25.4%	3.7 ±0.01	+5.7%	8.6 ± 0.2	+19.4%

nanofiller, PO, and Al_2O_3 NP loading levels. Across all epoxy samples, a noticeable upsurge in the COF was observed as the effective loads increased. However, in samples containing hybrid nanofillers, there was an apparent reduction in friction within the contact area. This phenomenon can be elucidated by the self-lubricating attributes of paraffin oil and the rolling effects of Al_2O_3 NPs, both of which had a discernible influence on the sliding conditions. As a result, it was shown that raising the hybrid nanofillers' loading amount caused the COF to gradually decrease [49]–[51]. This trend remained consistent across various loading levels. The most noteworthy reduction in the COF was achieved with epoxy NC3, containing a 1.0 wt. % loading of Al_2O_3 NPs, corresponding to a remarkable 43.7% improvement in COF reduction. The augmented COF in other cases, such as epoxy NC4 and NC5, could be ascribed to the higher loading of hybrid nanofillers, which introduced an opportunity of aggregating particles inside the substance's matrix. This agglomeration was proposed to restrict particle dispersion and shear transfers between layers. Moreover, Figure 6b demonstrates that the wear rate represents the volume loss for each sample was calculated using the empirically observed fluctuations in sample weight. The results reiterated the previously observed trend in friction behavior, illustrating a parallel pattern in wear rate. The findings demonstrated that the incorporation of hybrid nanofillers into the epoxy matrix significantly improved wear resistance. Under the sliding action, epoxy NC3, featuring a 1.0 wt. % loading of Al_2O_3 NPs, exhibited a wear rate reduction of approximately 34.1%, compared to the free epoxy matrix. This enhancement could be ascribed to the inclusion of hybrid fillers, including PO and Al_2O_3 NPs, which contributed to the creation of a lubricant film within the sliding contact interfaces [1], [71]. The aggregation of nanoparticles and poorly connected sliding planes were among the difficulties that emerged at high loading levels of fillers. Loading content of more than 1.0 weight percent of Al_2O_3 NPs limited internal molecule mobility, which could have resulted in permanent deformation.

The surfaces that had undergone wear were meticulously scrutinized to obtain more comprehension of the deformation and damage mechanisms taking place during sliding. To accomplish

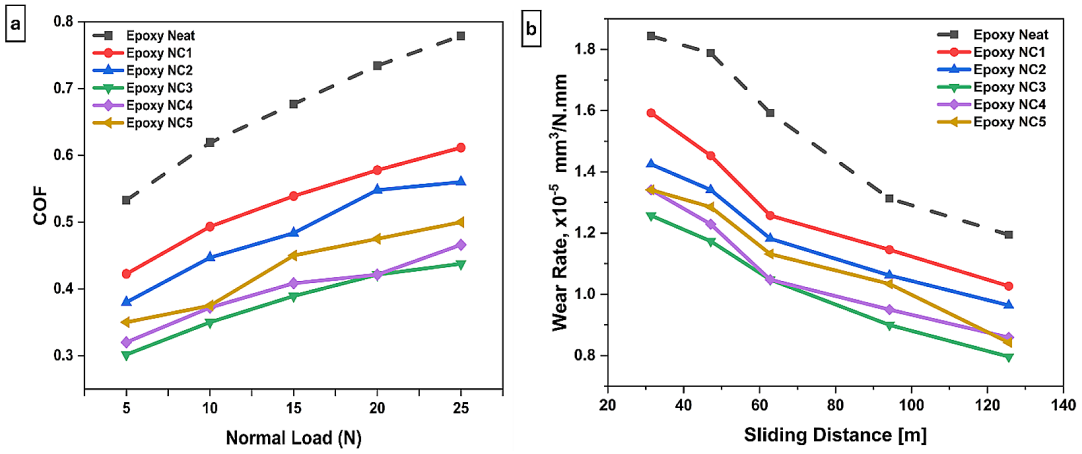

Figure 6. (a)The epoxy nanocomposites' friction coefficient, (b) the epoxy nanocomposites' wear rate

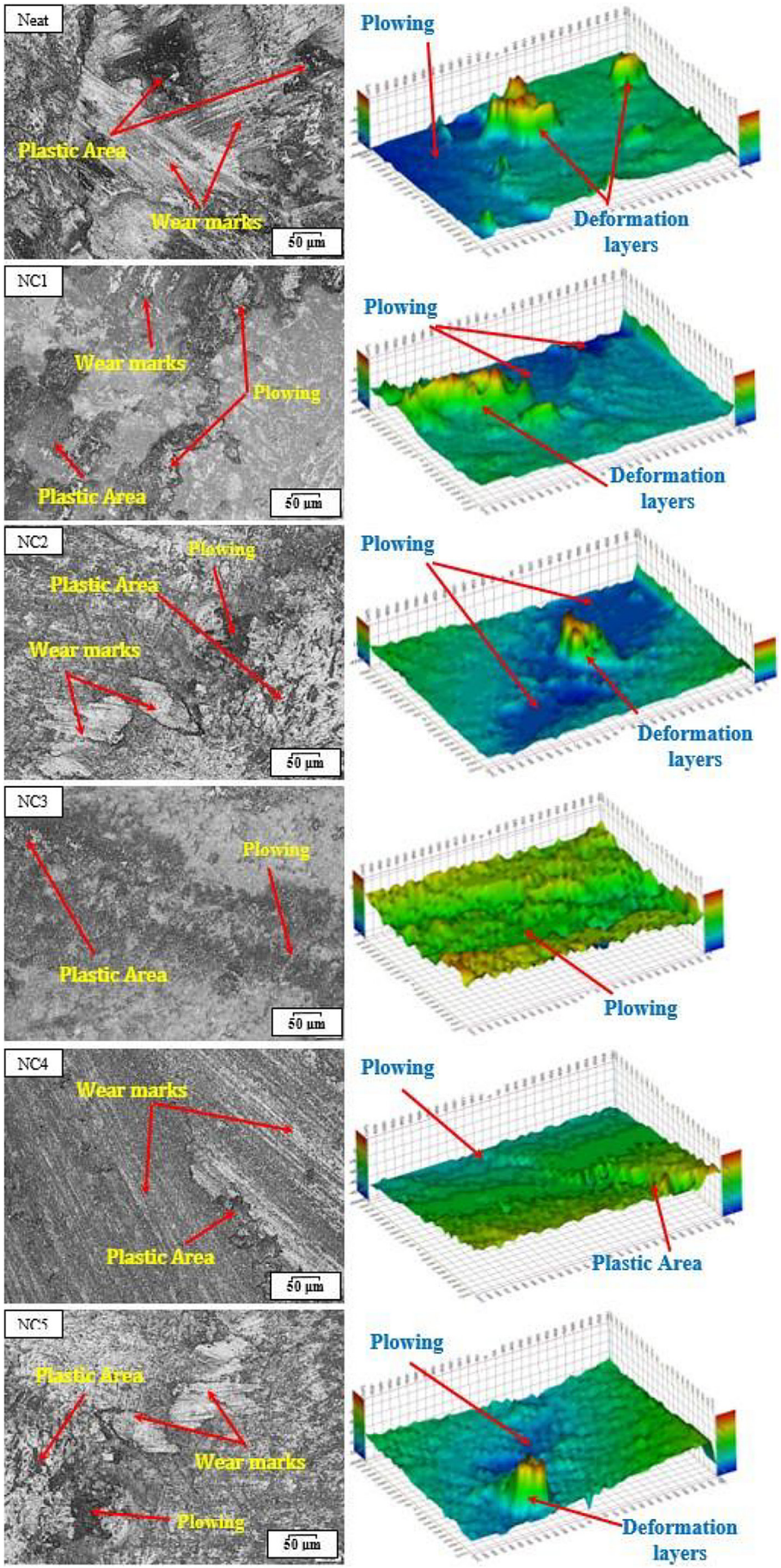

Figure 7. 2D and 3D topography optical images of samples of epoxy nanocomposites under wear

this, optical images of the surface topography and SEM micrographs were employed. Optical microscopy was employed to examine the topography of these worn surfaces, producing 2D and 3D scanned pictures, as indicated in Figure 7. The deteriorated surface of the basic epoxy sample (Neat) revealed apparent signs of damage, with layers of plastic deformation, large wear tracks, and plowing over the contact surfaces. Meanwhile, the topography photos of the nanocomposites revealed that the epoxy matrix had effectively dispersed hybrid fillers, preventing particle clumping and isolating the sliding interfaces. Specifically, for Sample epoxy NC1, the outer layer revealed grooves, wear paths, and a small plowing location, indicating minimized loss of mass as opposed to basic epoxy sample. Moreover, increasing the filling amount remained a favorable trend, with the surface of Sample epoxy NC2 exhibiting less damage than epoxy NC1. Sample epoxy NC3's surface showed less wear paths, cracks, and grooves and felt even smoother. Furthermore, wear scars and plowing site resurfaced on the epoxy NC4 and NC5 sample. A decreased wear rate may be deduced due to the epoxy matrix containing hybrid fillers enabled the creation of a self-lubricating film. Overloading this loading limit, however, was deemed inappropriate since it would impair wear and friction performance due to agglomeration and incoherence [73].

The structural mechanisms of the matrix and nanocomposites were examined and analysed using SEM images, as illustrated in Figure 8. The topography of the epoxy neat sample exhibited weak cohesion layers, marked by the presence of cracks and furrows. In contrast, samples reinforced with hybrid nanofillers exhibited improved interlayer cohesion and reduced structural discontinuities. The sample structure of epoxy NC1 appeared to be an improvement over the pure sample, however, upon closer examination of the image, it was clear that there were certain flaws such as furrows and voids on the surface. As can be seen in the SEM images of samples NC2 and NC3, the matrix structure notably improved with

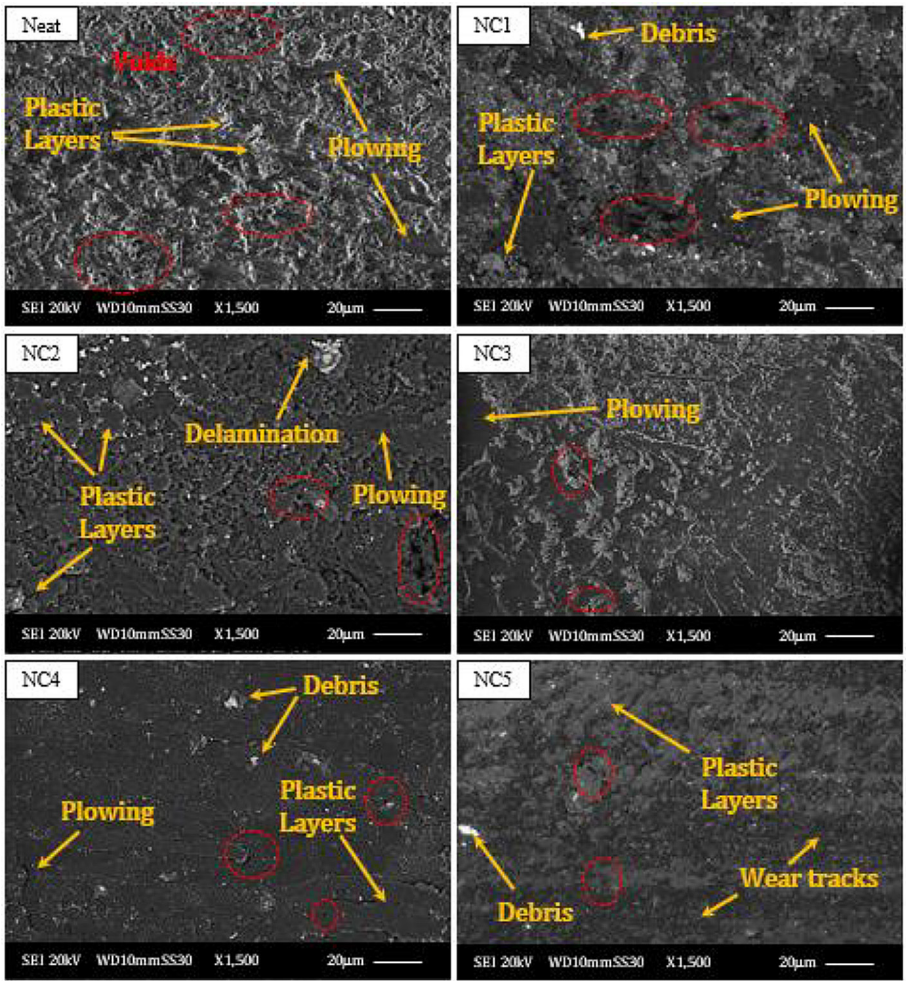

Figure 8. SEM pictures of the worn epoxy nanocomposite's surfaces

increasing loading amount, with cracks and voids decreasing. This enhancement indicates that the nanofillers, PO and Al_2O_3, enhanced the structure and the linkages between the layers in the matrix [71], [74]. Consequently, the incorporation of fillers inside the substrate successfully prevented cracks from spreading across the surface of the sample. However, an excessive amount of nanofillers led to agglomeration and inadequate particle dispersion, resulting in plastic flow at the sliding interface.

RSM analysis was performed to statistically simulate and optimize the epoxy resin manufacturing process, as dedicated in Figure 9. The 3D surface plots provide visual insights into the relationships between compositional variables and performance outcomes, highlighting linear and nonlinear interaction effects.

The effect of the epoxy matrix's loading level under different loads on the composite's behavior is illustrated in Figure 9a. A complex optimization environment is unique in analyzing the relationship as a surface with a saddle point topology. It may reveal the extent to which these two factors interact with changes in surface profiles. The results show that an increase in the applied load drives the coefficient of friction upwards. Furthermore, Sample Epoxy-NC3 exhibits the best frictional performance at each applied loading level. Figure 9b also illustrates the change in the wear rate according to the epoxy matrix loading level at different sliding distances. It is worth noting that increasing Al_2O_3 NPs loading content significantly affects the surface properties of the wear rate. The incorporation of Al_2O_3 NPs leads to a decrease in the COF and the wear rate, consistent with experimental observations.

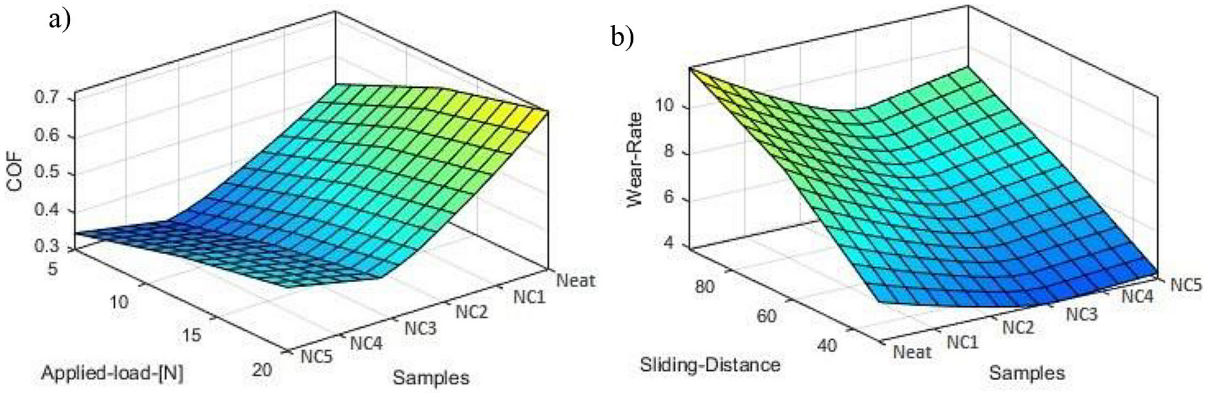

Figure 9. (a) Friction coefficient and wear rate in relation to change of normal load, (b) friction coefficient and wear rate in relation to change of rotational speed

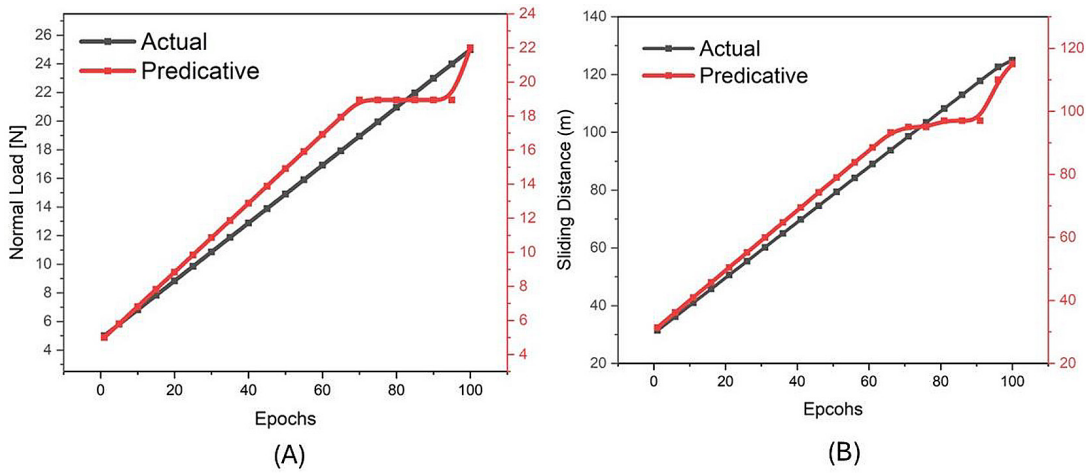

Figure 10. Comparison between actual and predictive data of training section with ANFIS predicted ones: (a) normal load, (b) sliding distance

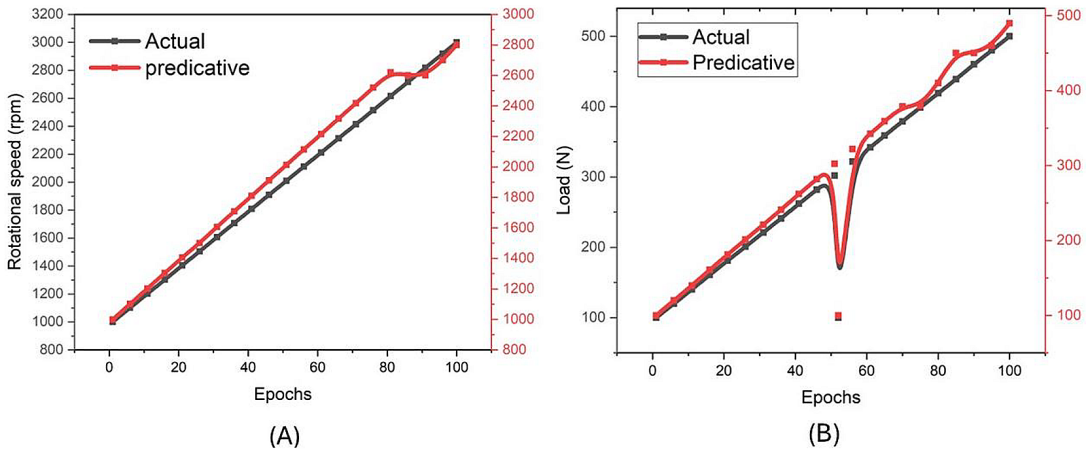

Figure 11. Comparison between actual and predictive data of detection section with ANFIS predicted ones: (a) rotational speed, (b) load

Dual-axis time series plots facilitate the comparison of machine learning models' performance by displaying the convergence of actual and anticipated values across training epochs. A strong model displays a close match between predictions and actual experimental values, indicating successful training, as depicted in Figure 10. The representation is particularly useful in materials science for multi-objective optimization, accommodating parameters with differing units. Additionally, the training dynamics highlighted in another plot show effective performance in predicting tribological properties, with most predictions showing steady enhancements, although some complexities arise, suggesting potential data outliers or model overfitting, as displayed in Figure 11. The ANFIS model emphasizes the importance of multi-factor interactions, revealing that factors like applied stress and sliding motion significantly impact epoxy matrix performance, showcasing ANFIS's efficacy in resin formula prediction and adjustment.

CONCLUSIONS

The current study presents an AI-driven multi-parameter optimization framework for developing high-performance epoxy nanocomposites reinforced with paraffin oil and Al_2O_3 NPs for tribological applications. The combined experimental investigation and predictive modeling demonstrate that the incorporation of hybrid nanofillers significantly improves mechanical properties, including yield strength, elastic modulus, and hardness, while effectively reducing the COF and wear rate. Importantly, the most favorable results in terms of the lowest COF and wear rate were attained when the loading content of Al_2O_3 NPs reached 1.0 wt.%, resulting in substantial reductions of approximately 43% and 34%, respectively. This intriguing outcome can be attributed to the dual role played by each nanofiller component. Paraffin oil played a pivotal role in forming a lubricating layer that effectively separated and shielded the sliding surfaces. However, agglomeration becomes evident at higher loading levels (≥1.5 wt.% Al_2O_3 NPs), above the optimal value of 1.0 wt.%., restricting motion between layers and subsequently leading to increased plastic deformation and frictional effects. Examination of worn surfaces, conducted through optical topography and SEM images, provided insights into the epoxy nanocomposite matrix structure. It was apparent that epoxy reinforced up to 1.0 wt.% of Al_2O_3 NPs exhibited a well-structured matrix with smoother surfaces and reduced voids. Consequently, the consistent distribution of fillers across the resin demonstrated efficacy in hindering the propagation of cracks. At higher loadings (≥1.5 wt.% Al_2O_3), particle agglomeration adversely affected performance, leading to increased plastic deformation and friction.

A major contribution of this work is the implementation of the Adaptive Neuro-Fuzzy Inference System as an intelligent predictive tool capable of capturing nonlinear relationships between composition variables and performance metrics. The model demonstrated strong agreement with experimental results, enabling reliable prediction and optimization of hardness, modulus, friction, and wear responses. This AI-assisted approach provides an efficient pathway for accelerating

materials design and reducing experimental trial and error.

Overall, the integration of hybrid nanofillers with AI-based optimization establishes a robust strategy for designing epoxy composites with enhanced tribological performance, offering practical potential for bearing and frictional components and contributing to the advancement of data-driven materials engineering.

REFERENCES

1. Bajpai A., Wetzel B., Klingler A., and Friedrich K., Mechanical properties and fracture behavior of high-performance epoxy nanocomposites modified with block polymer and core–shell rubber particles, J. Appl. Polym. Sci., 2020; 137(11), 48471.
2. Kinloch A. J., Mechanics and mechanisms of fracture of thermosetting epoxy polymers, in Epoxy resins and composites I, Springer, 2005, pp. 45–67.
3. Schut J. H., Nanocomposite do more with less, Plastics Technology, 2006; 52(2), 56–59.
4. Nabhan A., Sherif G., Abouzeid R., and Taha M., Mechanical and tribological performance of HDPE matrix reinforced by hybrid Gr/TiO2 NPs for hip joint replacement, J. Funct. Biomater., 2023; 14(3), 140.
5. Girish Chandran V. and Waigaonkar S. D., Mechanical properties and creep behavior of rotationally moldable linear low density polyethylene-fumed silica nanocomposites, Polym. Compos., Mar. 2017; 38(3), 421–430, https://doi.org/10.1002/PC.23600
6. A. Jayanthi et al., "Mechanical and tribological properties of TiC nano particles reinforced polymer matrix composites," Mater. Today Proc., Jan. 2022; 59, 1472–1477, https://doi.org/10.1016/j.matpr.2022.01.096
7. Nabhan A., Fouly A., Albahkali T., Shar M. A., Abdo H. S., and Taha M., Casting light on the tribological properties of paraffin-based HDPE enriched with graphene nano-additives: an experimental investigation, Mater. Res. Express, 2023; 10(12), 125301.
8. Alfattani R., Hassan M. K., Samy A. M., and Ameer A. K., Enhancing the Epoxy Flooring Materials to Avoid Dangerous of Electrostatic Charge and Slip Accidents, Solid State Technol, 2020; 63, 7756–7771.
9. A. K. Ameer, A. Khamaj, I. AMM, and A. M. Samy, "Enhancing the Safety of Epoxy Flooring Materials in Wet Working Condition," King Abdulaziz Journal: Engineering Sciences, 2022; 32(1), 58–68.
10. Hadidi H. M., Eldbari M. A., Hassan M. K., Samy A. M., and Ameer A. K., Frictional Behavior of self lubricated biocompatible polymeric Materials, KGK-Kautschuk Gummi Kunststoffe, 2022; 75(2), 66–72.
11. Rudnick L. R., Synthetics, mineral oils, and bio-based lubricants: chemistry and technology. CRC press, 2020.
12. Bakrey M., Nabhan A., Ameer A. K., and El-Sharkawy M. R., Performance of lithium-based grease filled with hybrid paraffin oil and TiO_2 nanoparticles for vehicle applications, International Journal of Vehicle Structures & Systems, 2023; 15(4), 540–546.
13. Rawat S. S., Harsha A. P., Chouhan A., and Khatri O. P., Effect of graphene-based nanoadditives on the tribological and rheological performance of paraffin grease, J. Mater. Eng. Perform., 2020; 29(4), 2235–2247.
14. Adhvaryu A., Erhan S. Z., and Perez J. M., Preparation of soybean oil-based greases: effect of composition and structure on physical properties, J. Agric. Food Chem., 2004; 52(21), 6456–6459.
15. Rawat S. S. and Harsha A. P., The lubrication effect of different vegetable oil-based greases on steel-steel tribo-pair, Biomass Convers. Biorefin., 2022; pp. 1–13.
16. Taha M., Khiari R., and Nabhan A., Structure—property relationships in HDPE nanocomposites reinforced with CNF and CNF-L: mechanical strength and tribological stability, Journal of King Saud University–Engineering Sciences, 2025; 37(8), 60.
17. Gupta R. N. and Harsha A. P., Antiwear and extreme pressure performance of castor oil with nano-additives, Proceedings of the Institution of Mechanical Engineers, Part J: Journal of Engineering Tribology, 2018; 232(9), 1055–1067.
18. Nabhan A. et al., Comparative Performance Analysis of Gear Oil Enhanced With Biomass-Derived Cellulose Nanocrystals and Al_2O_3 Nanoparticles, Int. J. Polym. Sci., 2025; 2025(1), 8850107.
19. Nabhan A., Rashed A., Taha M., Abouzeid R., and Barhoum A., Tribological performance for steel–steel contact interfaces using hybrid MWCNTs/Al_2O_3 nanoparticles as oil-based additives in engines, Fluids, 2022; 7(12), 364.
20. Taha M. et al., Utilizing cellulose nanofibers to enhance spent engine oil performance: a sustainable environmental solution, Results in Engineering, 2024; p. 102395.
21. Liu L. and Zhou W., MoS2 hollow microspheres used as a green lubricating additive for liquid paraffin, Tribol. Int., 2017; 114, 315–321.
22. Rajendran S. et al., Replacement of petroleum based products with plant-based materials, green and sustainable energy—a review, Engineering Reports, 2025; 7(4), e70108.
23. Khot S. N. et al., Development and application of triglyceride-based polymers and composites, J. Appl. Polym. Sci., 2001; 82(3), 703–723.
24. Kerton F. M., Applying the principles of green chemistry to achieve a more sustainable polymer life cycle, Curr. Opin. Green Sustain. Chem., 2025;

51, 100996.

25. Filiciotto L. and Rothenberg G., Biodegradable plastics: standards, policies, and impacts, ChemSusChem, 2021; 14(1), 56–72.
26. Bertani R., Bartolozzi A., Pontefisso A., Quaresimin M., and Zappalorto M., Improving the antimicrobial and mechanical properties of epoxy resins via nanomodification: an overview, Molecules, 2021; 26(17), 5426.
27. Zhang C., Garrison T. F., Madbouly S. A., and Kessler M. R., Recent advances in vegetable oil-based polymers and their composites, Prog. Polym. Sci., 2017; 71, 91–143.
28. Badran H., Hasan M. K., and Ali W. Y., Tribological Behavior of Epoxy Reinforced with Carbon Nano tubes and filled by Vegetables Oils, KGK-Kautschuk Gummi Kunststoffe, 2017; 70(11–12), 38–42.
29. Taha M., Fouly A., Abdo H. S., Alnaser I. A., Abouzeid R., and Nabhan A., Unveiling the Potential of Rice Straw Nanofiber-Reinforced HDPE for Biomedical Applications: Investigating Mechanical and Tribological Characteristics, J. Funct. Biomater., 2023; 14(7), 366.
30. Bazrgari D., Moztarzadeh F., Sabbagh-Alvani A. A., Rasoulianboroujeni M., Tahriri M., and Tayebi L., Mechanical properties and tribological performance of epoxy/Al_2O_3 nanocomposite, Ceram. Int., 2018; 44(1), 1220–1224.
31. Sprenger S., Epoxy resin composites with surface-modified silicon dioxide nanoparticles: A review, J. Appl. Polym. Sci., 2013; 130(3), 1421–1428.
32. Elshemy A. E., Showaib A. E., and Nabhan A., Erosive Wear of Surfaces Coating by Epoxy/TiO2 Nanocomposite, KGK-Kautschuk Gummi Kunststoffe, 2022; 75(4), 68–72.
33. Bello R. H., Coelho L. A. F., and Becker D., Role of chemical funcionalization of carbon nanoparticles in epoxy matrices, J. Compos. Mater., 2018; 52(4), 449–464.
34. Turaka S. and Bandaru A. K., Enhancement in mechanical properties of glass/epoxy composites by a hybrid combination of multi-walled carbon nanotubes and graphene nanoparticles, Polymers (Basel)., 2023; 15(5), 1189.
35. Singh S. K., Singh L. D., Vijay K., Sonker P. K., and Verma Y. K., Improved mechanical and tribological performance of GFRP laminate composites with TiO2–SiC hybrid fillers in modified epoxy matrix for automotive applications, Polym. Compos., 2025.
36. Nabhan A., Taha M., Ibrahim A. M. M., and Ameer A. K., Role of hybrid nanofiller GNPs/Al_2O_3 on enhancing the mechanical and tribological performance of HDPE composite, Sci. Rep., 2023; 13.
37. Nabhan A., Rashed A., Bettaieb F., Aboelhassan H. G., and Taha M., Advanced characterization of nanocellulose and its composites, in Properties and Characterization of Nanocellulose and Nanocellulose-Based Composites, Elsevier, 2026, pp. 475–503.
38. Cui J. et al., Nano-Al_2O_3 obtained the best tribological properties than similar hardness nanoparticles filled into epoxy resin," Colloid Polym. Sci., 2025; 303(5), 735–745.
39. Liu L. et al., Improving corrosion resistance of epoxy coating by optimizing the stress distribution and dispersion of SiO2 filler," Prog. Org. Coat., 2023; 179, 107522.
40. Venkataraman K. S., Friction and Wear Micro-mechanics of Epoxy Reinforced by Graphene Based Fillers, The Pennsylvania State University, 2022.
41. Dev B. et al., Graphene-alumina hybrid nanoparticle effects on the thermomechanical behavior of jute fiber/epoxy nanocomposites, Next Materials, 2026; 10, 101524.
42. Abbas S. S., Raouf R. M., and Al-Moameri H., A review of epoxy-nanocomposite properties, Journal of Engineering and Sustainable Development, 2024; 28(1), 76–95.
43. Patil Devansh P., and Pinjari D. V, Oil-based epoxy and their composites: a sustainable alternative to traditional epoxy, J. Appl. Polym. Sci., 2024; 141(29), e55560.
44. Karacor B. and Özcanlı M., A Short Review: The Use and Application of Matrix Resins Formed with Some Plant-Based Oils in Bio-Composite Materials, Düzce Üniversitesi Bilim ve Teknoloji Dergisi, 2024; 12(3), 1315–1333.
45. Ilyina S. O., Vlasova A. V., Gorbunova I. Y., Lukashov N. I., Kerber M. L., and Ilyin S. O., Epoxy phase-change materials based on paraffin wax stabilized by asphaltenes, Polymers (Basel)., 2023; 15(15), 3243.
46. Atta A. M., Mohamed N. H., Rostom M., Al-Lohedan H. A., and Abdullah M. M. S., New hydrophobic silica nanoparticles capped with petroleum paraffin wax embedded in epoxy networks as multifunctional steel epoxy coatings, Prog. Org. Coat., 2019; 128, 99–111.
47. Raymond M. and Bui V. T., Epoxy/castor oil graft interpenetrating polymer networks, J. Appl. Polym. Sci., 1998; 70(9), 1649–1659.
48. Sahoo S. K., Khandelwal V., and Manik G., Development of completely bio-based epoxy networks derived from epoxidized linseed and castor oil cured with citric acid, Polym. Adv. Technol., 2018; 29(7), 2080–2090.
49. Saikia A. and Karak N., Castor oil based epoxy/clay nanocomposite for advanced applications, Am. J. Eng. Applied Sci, 2016; 9, 31–40.
50. Bazrgari D., Moztarzadeh F., Sabbagh-Alvani A. A., Rasoulianboroujeni M., Tahriri M., and Tayebi L., Mechanical properties and tribological performance of epoxy/Al_2O_3 nanocomposite, Ceram. Int., 2018; 44(1), 1220–1224.

51. Dandan Doganci M. and Sevinç H., Investigation of superhydrophobic and anticorrosive epoxy films with Al2O3 nanoparticles on different surfaces, ACS Omega, 2023; 8(24), 21559–21570.
52. Jogesh K. S., Development of Vegetable Oil-Based Nano-Lubricants Using Ag, h-BN and MgO Nanoparticles as Lubricant Additives, The University of Texas Rio Grande Valley, 2022.
53. Das G. and Karak N., Vegetable oil-based flame retardant epoxy/clay nanocomposites, Polym. Degrad. Stab., 2009; 94(11), 1948–1954.
54. Khalil H. P. S. A., Fizree H. M., Bhat A. H., Jawaid M., and Abdullah C. K., Development and characterization of epoxy nanocomposites based on nano-structured oil palm ash, Compos. B Eng., 2013; 53, 324–333.
55. Xiong W., Li X., Chen X., Zhang C., and Luo J., Preparation and tribological properties of self-lubricating epoxy resins with oil-containing nanocapsules, ACS Appl. Mater. Interfaces, 2022; 14(16), 18954–18964.
56. Kibrete F., Trzepieciński T., Gebremedhen H. S., and Woldemichael D. E., Artificial intelligence in predicting mechanical properties of composite materials, Journal of Composites Science, 2023; 7(9), 364.
57. Mohit H. et al., Effect of bio-fibers and inorganic fillers reinforcement on mechanical and thermal characteristics on carbon-Kevlar-basalt-innegra fiber bio/synthetic epoxy hybrid composites, Journal of Materials Research and Technology, 2023; 23, 5440–5458.
58. Esfe M. H., Esmaily R., Mahabadi S. T., Toghraie D., Rahmanian A., and Fazilati M. A., Application of artificial intelligence and using optimal ANN to predict the dynamic viscosity of Hybrid nano-lubricant containing Zinc Oxide in Commercial oil, Colloids Surf. A Physicochem. Eng. Asp., 2022; 647, 129115.
59. Ragupathy K., Velmurugan C., Ebenezer Jacob Dhas D. S., Senthilkumar N., and Leo Dev Wins K., Prediction of dry sliding wear response of AlMg1SiCu/silicon carbide/molybdenum disulphide hybrid composites using adaptive neuro-fuzzy inference system (ANFIS) and response surface methodology (RSM), Arab. J. Sci. Eng., 2021; 46(12), 12045–12063.
60. Fouly A., Taha M., Albahkali T., Shar M. A., Abdo H. S., and Nabhan A., Developing Artificial Intelligence Models for Predicting the Tribo-Mechanical Properties of HDPE Nanocomposite Used in Artificial Hip Joints, IEEE Access, 2024; 12, 14787–14799.
61. Singh K. P., Singh A., Kumar N., and Tripathi D. N., Morphological features, dielectric and thermal properties of epoxy–copper cobaltite nanocomposites: preparation and characterization, Bulletin of Materials Science, 2020; 43, 1–10.
62. Kanimozhi K., Sethuraman K., Selvaraj V., and Alagar M., Development of ricehusk ash reinforced bismaleimide toughened epoxy nanocomposites, Front. Chem., 2014; 2, 65.
63. Velmurugan R. and Mohan T. P., Room temperature processing of epoxy-clay nanocomposites, J. Mater. Sci., 2004; 39, 7333–7339.
64. Tomić M. et al., Polyamidoamine as a clay modifier and curing agent in preparation of epoxy nanocomposites, Prog. Org. Coat., 2019; 131, 311–321.
65. Naous W., Yu X., Zhang Q., Naito K., and Kagawa Y., Morphology, tensile properties, and fracture toughness of epoxy/Al_2O_3 nanocomposites, J. Polym. Sci. B Polym. Phys., 2006; 44(10), 1466–1473.
66. Fouly A. and Alkalla M. G., Effect of low nanosized alumina loading fraction on the physicomechanical and tribological behavior of epoxy, Tribol. Int., 2020; 152, 106550.
67. Panda P., Mishra G., Mantry S., Singh S. K., and Sinha S. P., A study on mechanical, thermal, and electrical properties of glass fiber-reinforced epoxy hybrid composites filled with plasma-synthesized AlN,"J. Compos. Mater., 2014; 48(25), 3073–3082.
68. Zhao H. X. and Li R. K. Y., Effect of water absorption on the mechanical and dielectric properties of nano-alumina filled epoxy nanocomposites, Key Eng. Mater., 2007; 334, 617–620.
69. Zhao H. and Li R. K. Y., Effect of water absorption on the mechanical and dielectric properties of nano-alumina filled epoxy nanocomposites, Compos. Part A Appl. Sci. Manuf., 2008; 39(4), 602–611.
70. Satapathy A., Jha A. K., Mantry S., Singh S. K., and Patnaik A., Processing and characterization of jute-epoxy composites reinforced with SiC derived from rice husk, Journal of Reinforced Plastics and Composites, 2010; 29(18), 2869–2878.
71. Verma V. and Tiwari H., Role of filler morphology on friction and dry sliding wear behavior of epoxy alumina nanocomposites, Proceedings of the Institution of Mechanical Engineers, Part J: Journal of Engineering Tribology, 2021; 235(8), 1614–1626.
72. Ji Q. L., Zhang M. Q., Rong M. Z., Wetzel B., and Friedrich K., Friction and wear of epoxy composites containing surface modified SiC nanoparticles, Tribol. Lett., 2005; 20, 115–123.
73. Maghsoudlou M. A., Isfahani R. B., Saber-Samandari S., and Sadighi M., Effect of interphase, curvature and agglomeration of SWCNTs on mechanical properties of polymer-based nanocomposites: Experimental and numerical investigations, Compos. B Eng., 2019; 175, 107119.
74. Bazrgari D., Moztarzadeh F., Sabbagh-Alvani A. A., Rasoulianboroujeni M., Tahriri M., and Tayebi L., Mechanical properties and tribological performance of epoxy/Al_2O_3 nanocomposite, Ceram. Int., 2018; 44(1), 1220–1224.